Spontaneous Nanoripple Formation on Metallic Templates

Paula Cecilia dos Santos Claro, Marcos Federico Castez, Patricia Laura Schilardi, Noelia Beatriz Luque,[†] Ezequiel Pedro Marcos Leiva, and Roberto Carlos Salvarezza*

Instituto de Investigaciones Fisicoquímicas Teóricas y Aplicadas (INIFTA), Facultad de Ciencias Exactas, Universidad Nacional de La Plata, CONICET, Sucursal 4 Casilla de Correo 16, 1900 La Plata, Argentina. [†]Current address: Unidad de Matemática y Física, Facultad de Ciencias Químicas, Universidad Nacional de Córdoba, Argentina.

ABSTRACT Nanoripple structures spontaneously formed at room temperature during chemical and electrochemical deposition of metals, semiconductors, and alloys on gold and copper templates, patterned with nanocavities, have been studied by atomic force microscopy (AFM) and scanning tunneling microscopy (STM). Annealing the templates at ≈373 K also results in ripple formation. Both experimental results and modeling, including anisotropic surface diffusion, demonstrate that nanocavity size in the template determines the ripple wavelength and amplitude, prior to a final stage of coarsening. Therefore, an ordered array of "nanodefects" introduced in the substrate is able to guide the self-organization of these nanofeatures during their growth, creating the possibility for nanofabrication of parallel interconnections with adjustable periodicity. Ripples are robust nanostructures that can in turn be used as templates for the preparation of hybrid nanostructured surfaces with specific physical properties.

KEYWORDS: nanofabrication · templates · self-organized nanostructures · nanoripples · surface diffusion

The design and development of novel and reproducible strategies for nano- and microscale patterning of material surfaces has become one of the most relevant topics in emerging nanotechnology.[1] Nanofeatures synthesized on solid surfaces hold promise for unprecedented functionality. In order to achieve this goal, many patterning methods with different degrees of accuracy have been developed during the past decade.[2] One alternative to the conventional hard lithographic techniques for patterning materials, soft lithography, has provided many simple routes to fabricate different types of architectures in a simple and effective way.[3]

One of the key points in nanopatterning is related to the shape evolution of the small structures and how different physical processes, such as surface diffusion, surface tension, and deposition rate, or topographical features, such as small defects on the substrate, could affect their shape and stability. In fact, if we want to exploit the potential of nanostructured systems, first, we need a thorough understanding of the creation and evolution of geometrical features at this level. However, understanding fundamental phenomena leading to the formation, stability, and morphological evolution of nanoscale features is still lacking since, as dimensions shrink into the nanoscale, many classical macroscopic models for morphological evolution lose their validity.[4]

Miniaturization of technologies highlights special approaches such as self-organization of nanostructures. In particular, self-organized nanoripples have attracted considerable attention not only due to interesting physical properties related to their anisotropy but also as templates for growing other specific nanostructures.[5]

Ripple formation has been reported during deposition of different materials: Si by molecular beam epitaxy (MBE) and vapor phase epitaxy on Si(001),[6] GaAs by MBE and metal organic chemical vapor deposition on GaAs(110)[7−9] and on GaAs(001),[10,11] InP on InP by metal-organic MBE,[12] and (211) CdTe on Si by MBE.[13] Anisotropic surface diffusion of atoms has been considered as the main contribution for ripple formation in these systems. Ripple formation has also been reported on sputtered Si(001),[14] Ge(001),[15] Au(111),[16] Cu(110),[17] Ag(110),[18] and Al thin films.[19] A continuum equation, which includes both surface curvature-dependent erosion and diffusion terms, accounting for surface anisotropy and Ehrlich−Schwoebel barriers, has been proposed to explain the observed morphologies.[17,20]

Recently, we have studied silver electrodeposition on metallic templates with ordered arrays of nanocavities.[21] In this case, the nanocavities act as reactors where nucleation starts to form silver nanodots. However, further addition of small amounts

*Address correspondence to robsalva@inifta.unlp.edu.ar.

Received for review April 7, 2008 and accepted November 03, 2008.

Published online November 18, 2008.
10.1021/nn800212w CCC: $40.75

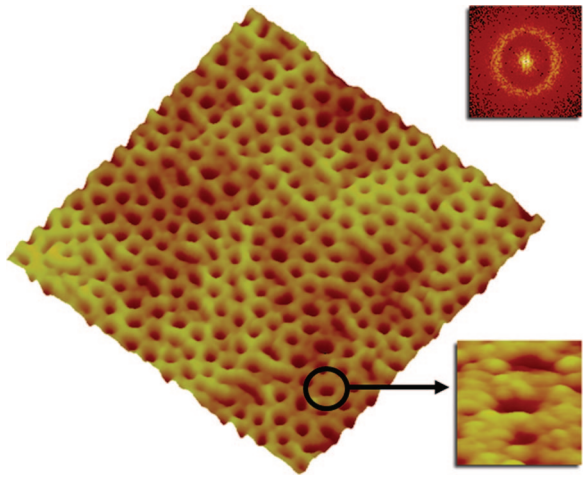

Figure 1. Three-dimensional AFM image (1 × 1 μm², pitch 60°) of a polycrystalline Au template. Inset on the top: fast Fourier transformation (FFT) of the corresponding 2D image. Inset on the bottom: 3D AFM image (75 × 75 nm², pitch 30°) of the nanocrystals at the template surface.

of material produces self-organization to a ripple structure that coarsens with time.

Here, we demonstrate that the formation of rippled structures is also a general phenomenon when metals, alloys, and semiconductors are deposited by different chemical methods (chemical reaction, electrochemistry) on ordered arrays of surface defects such as nanocavities. We also show that anisotropic surface diffusion accounts for the formation of well-ordered ripples extending over several microns.

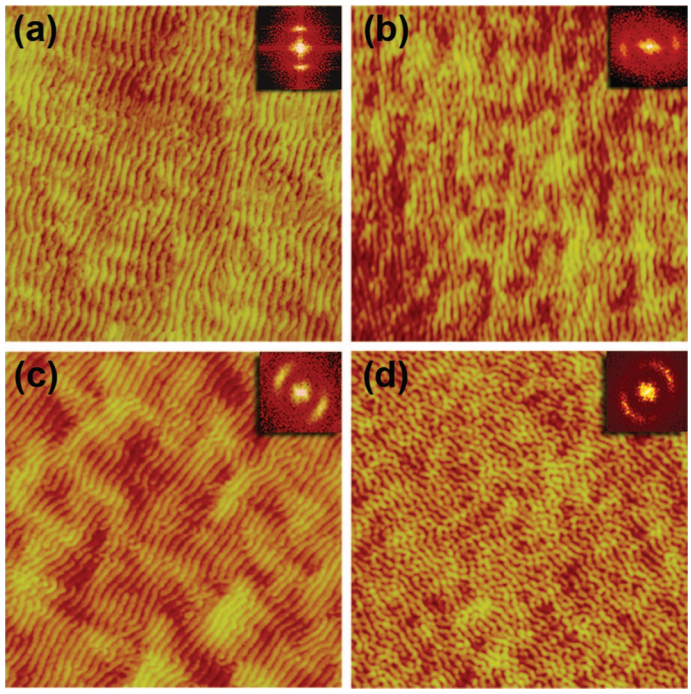

Figure 2. Two-dimensional images (2 × 2 μm²) of rippled structures grown on nanostructured templates and their corresponding FFT. (a) STM, electrodeposited Cu on a Au template; (b) AFM, electrodeposited Ag on a Au template; (c) STM, electrodeposited NiFeCo alloy after detachment from the Au template; (d) AFM, chemically formed CuS on a Cu template.

RESULTS AND DISCUSSION

Experimental Results. A typical AFM image of the metal templates used in this work, that is, the face of the deposit which was in contact with the silicon master surface,[22] reveals nanocavities of ~45 nm in diameter and 6 nm in depth (Figure 1).[23] The Fourier transform of the image (Figure 1, top inset) is consistent with a random array of defects with a short-range order of ~48 nm. AFM images at higher resolution (Figure 1, bottom inset) show that the template surface is formed by small grains of 10−20 nm in size.

Typical AFM images and the corresponding Fourier transforms of the rippled structures formed by deposition for four different systems (a−d) are shown in Figure 2. The ripple wavelength is ~50 nm with average amplitude of 4 nm, indicating a close relation with the nanocavity dimensions present in the template. In fact, the Fourier periods shown in Figure 2 are consistent with the ripple wavelength. Ripple formation starts simultaneously everywhere on the surface. Bifurcations are observed where out-of-phase ripples meet those originated at different locations. In all cases, the rippled structures were stable at room temperature during weeks, as observed for other metallic ripples.[18]

Evidence of how ripples are formed on these substrates is shown in Figure 3a for the copper sulfide formation on a copper template (system d). As recently reported for this system,[23] the nanocavities act as preferred nucleation centers of CuS nanocrystals that finally emerge from the cavities (circle in Figure 3a). At this stage, the nanocavities efficiently act as nanoreactors. However, with further material addition, the nanocrystals start to elongate in a preferred direction, as clearly shown in the STM image (arrow in Figure 3a). Finally, they merge forming ripples (Figure 2d).

Figure 3b shows how electrodeposited ripples evolve in system (b), as more mass is deposited when the deposition potential changes from $E = -0.02$ to -0.04 V (*vs* Ag^+/Ag). We observe that the ripple wavelength increases from 59 to 80 nm, concurrent with a slight increase in amplitude from 3 to 5 nm.

From these figures, it is evident that the aspect ratio changes from 0.05 to 0.06; therefore, the ripple formation can be described as a quasi-2D process involving the following stages: (1) preferred nucleation at nanocavities leading to nanodots, (2) ripple formation by merging of nanodots, with initial wavelength and amplitude being determined by the nanocavity size, and (3) ripple growth, resulting mainly in wavelength increase.

Important conclusions can be drawn from the images shown in Figure 3. The first one is that the nanodots are stable only in a narrow range of time, mass, or temperature. In fact, we also observe that even the array of gold nanocavities transforms into well-defined arrays of ripples after annealing at $T = 384$ K during 1 h (Figure 3c). The second one is that these nanoripples

are robust structures at room temperature that can be used as templates for large-scale production of mesoscale aligned nanostructures with adjustable periodicity.[24,25] Finally, the fact that annealing the template at relatively low temperatures induces the nanocavities to transform into ripples strongly indicates that surface diffusion plays a relevant role in this process.

Recently, we have shown[21] that the surface free energy of an array of circular structures is larger than that of an array of stripes with similar mass and diameter when the surface coverage by the circular structures reaches a critical value of ≈1/3. This is the driving force for the transition from nanodots to nanoripples observed during our deposition process. However, thermodynamics cannot explain the preferred orientation of the ripples over micron distances. Therefore, kinetic considerations should be involved in the self-organization of these systems. In this sense, we have implemented a two-dimensional lattice-gas model to simulate particle diffusion on a surface decorated with defects. Such defects mimic the nanocavities existing on the gold or copper templates in the experimental counterpart. Eventually, these defects can turn into preferential nucleation centers. As was pointed out above, results concerning template annealing imply that surface diffusion plays a main role in our system. As surface diffusion is an intrinsically conservative process, we have implemented conservative dynamics in our modeling. Note that other possible nonconservative processes are not expected to have an important contribution to the kinetic evolution. For instance, evaporation is not included in our model because it does not play a significant role at room temperature.[26,27]

It is evident that such a model does not attempt to describe closely the real experimental situation since it has been implemented by means of a simple dynamic rule on a two-dimensional substrate. Nevertheless, the use of a 2D model can be considered a reasonable approximation because the aspect ratio of the nanostructures, as discussed above, is small enough and only increases slightly with the depositing mass. Moreover, note that as it has been reported in ref 21, ripple formation was observed only after filling the nanocavities of the template. We will show that, in spite of its simplicity, a careful analysis of the model will be useful to understand several phenomena, such as the role of anisotropic surface diffusion in the formation of ripples and the influence of nanocavity geometry on the morphology of ripples from a qualitative point of view. Model details will be given in the following section.

Description of the Model: Let us consider a rectangular two-dimensional lattice of sizes L_x and L_y (in lattice units) along the x and y directions, respectively. On this two-dimensional array, we define a "matrix of defects" d_{ij}, which is a spin-like variable taking only one of two possible values: 0 and 1. Conventionally, we will as-

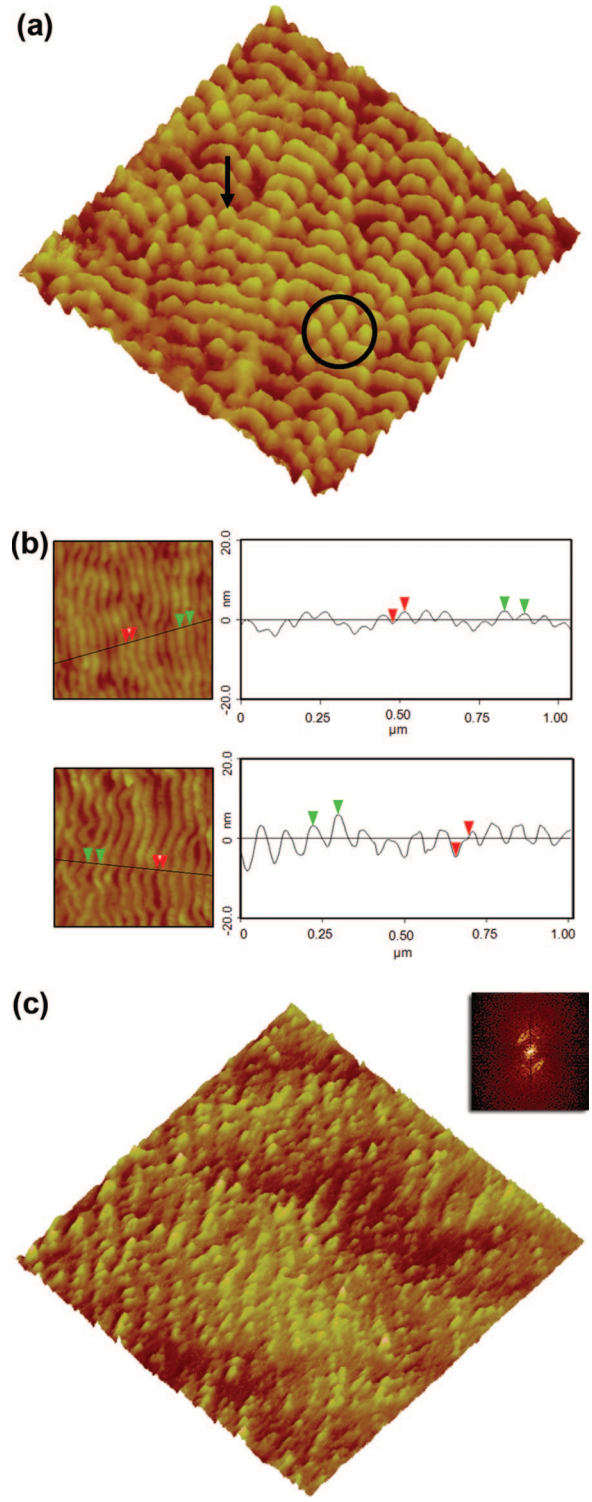

Figure 3. (a) Three-dimensional STM image (1 × 1 μm², pitch 60°) of CuS on a Cu template. The circle indicates preferred nucleation centers that form the nanodots, and the arrow shows the initial stage of ripple formation. (b) AFM results for silver electrodeposited on Au nanopatterns at different deposition potentials: Top: $E = -0.02$ V (*vs* Ag^+/Ag). Bottom: $E = -0.04$ V (*vs* Ag^+/Ag). AFM pictures are shown on the left, while cross-section profiles are given on the right. Green arrows are helpful to obtain the ripples wavelength, while red arrows denote the amplitude. Note that in the case of $E = -0.02$ V, the wavelength and amplitude are 59 and 3 nm, respectively, while for $E = -0.04$ V, the wavelength is 80 nm and the amplitude is 5 nm. (c) Three-dimensional STM image (1 × 1 μm², pitch 60°) of Au template with nanocavities after annealing at $T = 384$ K, the formed ripples have a wavelength of ~72 nm. Inset: FFT of 2D image corresponding to (c).

sume that $d_{ij} = 1$ implies that the site (i,j) is on a defect, while $d_{ij} = 0$ corresponds to a nondefect site (i,j). Throughout this work, we have initially considered matrices d_{ij} that correspond to periodic arrays of defects, such as periodic array of circular defects. We have then extended our results to random defect distributions.

Over the defect-covered lattices, there are particles that can diffuse, interacting among each other and interacting also with the substrate and with the defects, with different strengths. This lattice gas can be described, as is usual,[28,29] in terms of another spin-like variable S_{ij} that takes the value 1 if the site (i,j) is occupied, while $S_{ij} = 0$ on empty sites. The interaction particle−particle, particle−substrate, and particle−defect are introduced by means of the following Hamiltonian:

$$H = E_b \sum_{<i,j,l,m>} S_{ij}S_{lm} + E_s \sum_{i,j} S_{ij}(1 - d_{ij}) + E_d \sum_{i,j} S_{ij}d_{ij}$$

where $<>$ denotes a nearest neighbor restricted sum, E_b can be thought as the particle−particle interaction energy, while E_s and E_d are the particle−substrate and particle−defect interaction energies, respectively. Through this work, we have fixed $E_b = -0.1$ eV, $E_s = -0.1$ eV, and $E_d = -0.5$ eV (of course, negative energies correspond to attractive interactions); that is, particles can attach either at defects or elsewhere. Thus, particles interact strongly with defects, promoting nuclei formation at these sites. The nuclei then can grow by lateral attachment of particles.

The dynamical model rule by which a defect remains a favored attachment site during the whole evolution, even after the original cavity has been filled by the diffusing species, can be justified in our 2D approximation if one takes into account that the nuclei edges provide more coordination for arriving adatoms than the substrate sites.

The dynamic evolution of the model has been implemented in the spirit of the so-called "Kawasaki dynamics"[30,31] that is a type of dynamics in which the total number of particles is conserved, thus becoming useful to be implemented in lattice-gas systems. In Kawasaki dynamics, the probability amplitude for a transition from a state c_i into a configuration c_f is given by

$$w_k(c_i, c_f) = \frac{\exp(-\Delta E/2k_BT)}{\exp(-\Delta E/2k_BT) + \exp(\Delta E/2k_BT)}$$

and, so defined, Kawasaki dynamics satisfy the detailed balance condition for a Boltzmannian equilibrium state.

We have incorporated anisotropic diffusion in our model by introducing a parameter p $(0 \leq p \leq 1)$ that controls diffusion rates in the x and y directions. The case $p = 0.5$ corresponds to isotropic diffusion, while $p < 0.5$ $(p > 0.5)$ produces enhanced diffusivity along the y (x) direction.

From an algorithmic point of view, a diffusion attempt in the model proceeds as follows: A site (i,j) on the lattice is randomly chosen, and a diffusion direction is choose with probability p for a diffusion path along the x direction, while $1 - p$ is the probability that the diffusion event takes place along the y direction. Once the lattice site and the diffusion direction have been chosen, one of the two nearest neighbors of the site in the resulting preferred diffusion direction is randomly selected. If both the selected site is occupied and the selected nearest neighbor site is empty, the diffusion event takes place. In any other case, the diffusion event becomes frustrated and a new diffusion attempt is performed. $L_x \times L_y$ diffusion attempts correspond to one Monte Carlo Step (MCS) that will be used as a time unit throughout this work. It is worth mentioning that our model assumes a diffusion-controlled system evolution in which time scales associated with particle attachment and particle diffusion are decoupled. In this sense, simulated time measured in MCS is associated with the surface diffusion process. Although Kawasaki dynamics is not a real time scheme, it correctly describes the long time limit that concerns us.

Numerical Results: In this section, we present results obtained by a computer implementation of the model described in the previous section. As has been discussed in a recent paper,[21] the experimentally observed transition from nanodots into nanoripples can be understood by thermodynamical considerations since rippled structures have a lower free energy than a dotted configuration at intermediate coverages. Nevertheless, experimentally observed ripples have a preferred orientation; that is, ripple formation implies a spontaneous symmetry breaking.

To try to understand the possible mechanisms that promote this symmetry breaking, we have performed computer simulations on the Monte Carlo model introduced in the previous section. Figure 4 shows snapshots corresponding to the configuration of the system after an equilibration time of 5.10^5 MCS in the case of isotropic diffusion at 300 K, starting from a random initial condition and for different values of the coverage C. It can be seen that for a coverage $C = 0.5$ (Figure 4, top) nearly circular clusters and small elongated clusters coexist in the equilibrium state, while at $C = 0.7$ (Figure 4, middle) dots and small elongated clusters begin to coalesce to form larger structures. When the coverage is subsequently increased at $C = 0.9$ (Figure 4, bottom), the elongated structures are completely interconnected, forming a web, with holes localized in regions between defects. It is evident from Figure 4 that the case of isotropic diffusion ($p = 0.5$) gives rise to elongated structures to same extent (in a statistical sense) disposed along the x and y directions; so we can conclude that isotropic diffusion in our model does not

Figure 4. Snapshots at different coverages after an equilibration time of 5.10^5 MCS at 300 K in the case of isotropic diffusion ($p = 0.5$). The formation of elongated structures with no preferential orientation is observed. Lattice parameters are $L_x = 300$, $L_y = 300$, and the defect grid consists of a rectangular array of circles of diameter 10 lattice units and centers separated by 20 lattice units. Axes scales along x and y directions are linear in the range 0−300 in arbitrary units for all the simulated snapshots shown throughout this work.

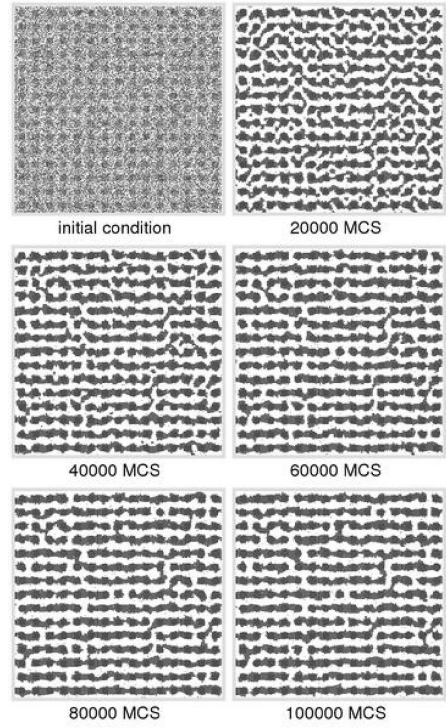

Figure 5. Snapshots showing the time evolution of a single system evolving at 400 K in the case of anisotropic diffusion ($p = 0.2$) on a defects covered lattice. The developing of ripples with a preferential orientation can be clearly seen. Lattice parameters are $L_x = 300$, $L_y = 300$, and the defect grid consists of a rectangular array of circles of diameter 10 lattice units and centers separated by 20 lattice units.

drive the system to any symmetry breaking. Thus, we consider anisotropic diffusion as a mechanism capable of explaining the symmetry breaking observed experimentally.

Spontaneous formation of ripples with a preferential orientation in the case of anisotropic diffusion ($p = 0.2$) in the model can be observed in Figure 5. In fact, starting from an initial random condition at a coverage $C = 0.5$, Figure 5 shows snapshots taken at successive times in the dynamic evolution (corresponding MCS are indicated below each snapshot). From this sequence, it is evident that anisotropic diffusion ($p = 0.2$, diffusion faster along the y direction) makes the system evolve from a random configuration into a rippled structure mostly disposed along the x direction (direction associated with a slower diffusion rate).

The proposed mechanism of dynamic evolution in the experimental system, that is, nucleation at nanocavities → growth of nuclei → dot formation → ripple formation → ripple coalescence, can be recovered in our model by considering equilibrium configurations at different coverages. In this way, we show in Figure 6 snapshots at different coverages corresponding to the state of the system after an equilibration period of 5.10^5 MCS at 400 K, starting from an initial random distribution of particles, and in the case of anisotropic diffusion ($p = 0.2$). At small coverages ($C = 0.1$), nuclei formation on defects can be seen (Figure 6 at the top on the left), and successive snapshots in Figure 6 at higher coverages show nuclei growth forming a dotted structure in which dots are wrapping the defects. Ripple formation and ripple coalescence are shown in Figure 6 for $C = 0.5$ and 0.6, respectively.

Comparing experimental and simulated templates, it is clear that the distribution of nanocavities in the experimental templates (see Figure 1) is more disordered. Thus, it is convenient to study how our numerical results are affected by introducing disorder in the array of defects. As is shown in Figure 7, on a template with a randomized array of circular defects (Figure 7, left), an initially random configuration ($C = 0.5$) of adatoms evolve into a rippled structure in the case of anisotropic diffusion ($p = 0.2$). It is evident (comparing Figures 6 and 7) that the disorder in the array of defects on the template also promotes a certain degree of disorder in the resulting rippled structure since resulting ripples are not so rectilinear. However, the relevant results we can extract from these simulations are that disorder in the model does not inhibit ripple formation and, as we shall show below, disorder does not change the harmonic content present in the rippled structure.

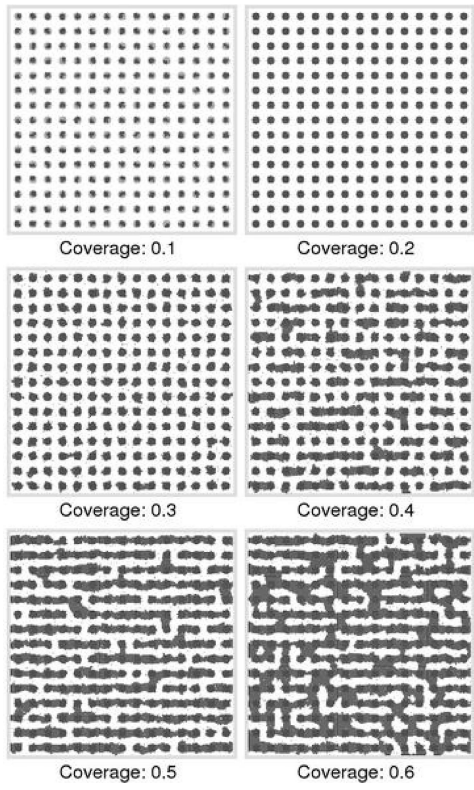

Figure 6. Snapshots at different coverages after an equilibration time of 5.10^5 MCS at 400 K in the case of anisotropic diffusion ($p = 0.2$) on a lattice covered with defects. When the coverage is increased, successive snapshots show nucleation on defects, growth of these nuclei, ripple formation, and ripple coalescence. Lattice parameters are $L_x = 300$, $L_y = 300$, and the defect grid consists of a rectangular array of circles of diameter 10 lattice units and centers separated by 20 lattice units.

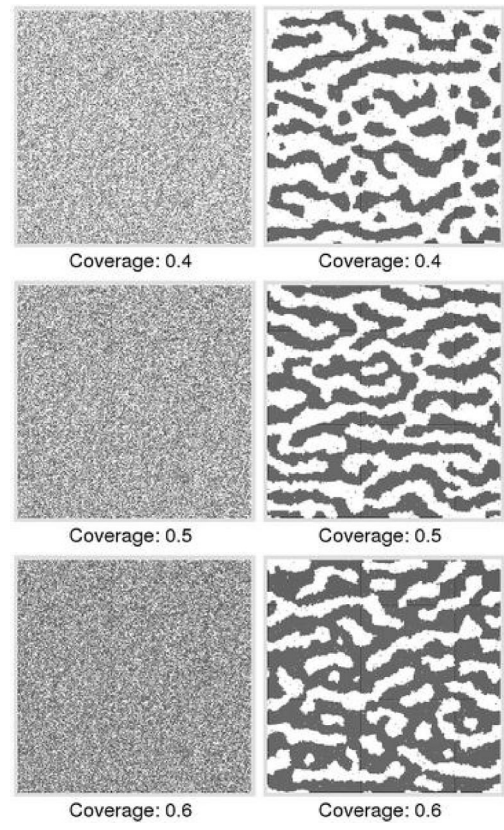

Figure 8. System evolution starting from a random initial condition (left panels) for different coverages after an equilibration time of 5.10^5 MCS at 400 K in the case of anisotropic diffusion ($p = 0.2$) on a defect-free lattice (right panels). Lattice parameters are $L_x = 300$ and $L_y = 300$.

It is evident from Figures 5−7 that the geometrical properties of ripples for intermediate coverages, such as ripple size and orientation, are strongly dependent on the defects array. In fact, defects act as "anchors" for ripple formation, breaking the lattice spatial homogeneity and, in this way, affecting the resulting geometry of ripples. Thus, potential wells provided by defects have an important role as "ripples organizers", promoting ripples with an almost constant width and nearly parallel among each other. This effect can be better appreciated by considering the case in which the system evolves in the absence of defects (*i.e.*, particles diffusing on a homogeneous lattice with no potential well). In this way, Figure 8 shows the evolution of the system for three different coverages, starting from a random initial condition (Figure 8, left) and after 5.10^5 MCS of evolution at 400 K (Figure 8, right) in the case of anisotropic diffusion ($p = 0.2$).

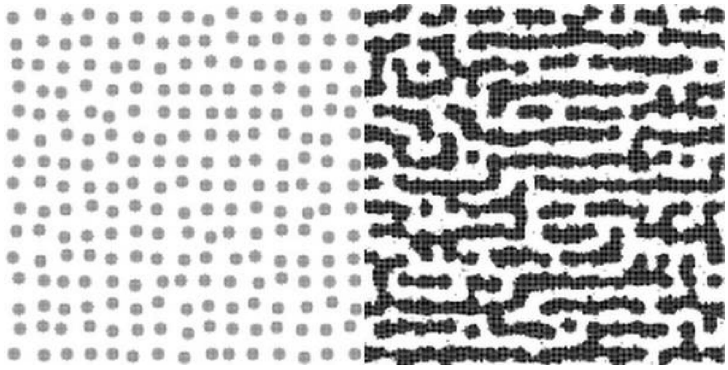

Figure 7. Left: Snapshot of a lattice covered with a randomized array of circular defects resembling the experimental templates. Right: Structures developed after an equilibration time of 5.10^5 MCS at 400 K in the case of anisotropic diffusion ($p = 0.2$) over the lattice of defects shown on the left, starting from a randomly disposed configuration of adatoms ($C = 0.5$). Lattice parameters are $L_x = 300$, $L_y = 300$, and the defect grid consists of a rectangular array of circles of diameter 10 lattice units and centers separated by 20 lattice units. The centers of the circles are displaced in a random amount from the fully symmetric situation.

Although the formation of ripples in the case shown in Figure 8 is evident, it is also clear that such ripples have lost their typical length scale (the ripple width) determined by the defects. In fact, the ripples' width is not nearly constant and their shapes are rather wavy. Characteristic length scales present in the rippled structures found in all considered cases (ordered defects, disordered defects, and no defects) are compared in Figure 9 (at the bottom) by means of a discrete Fourier transformation (DFT) of the corresponding averaged cross sections. In Figure 9 (at the top), we also show the characteristic length scales associated

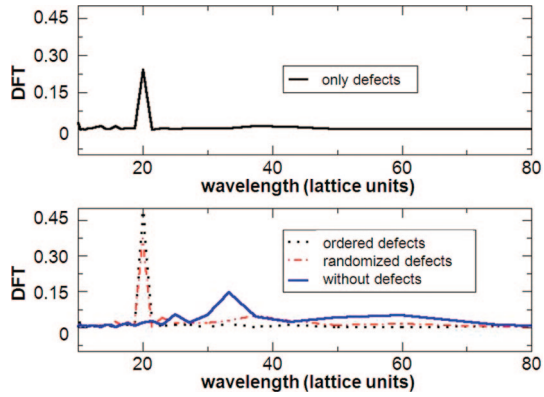

Figure 9. Top: Discrete Fourier transform of the averaged cross section associated with the randomized array of defects shown in Figure 7. Bottom: Discrete Fourier transform of the averaged cross sections of the rippled structures found in the cases of ordered defects, disordered defects, and without defects, all them under identical conditions as those described in the corresponding Figures 6−8.

with the array of defects for comparison purposes. It is clear from the analysis of the Figure 9 that the characteristic ripple length is strongly influenced by the presence of defects.

We will now justify one of the simplifications of our model. Mainly, that grain boundaries of the template can introduce a diffusion barrier to the adatoms.[32] For submicrometer sized grains where this barrier is present, roughening of the growing film takes place, leading to mound formation at grains while the grain boundary network remains unchanged.[32] Clearly, this is not our case since no significant roughening is observed (the ripple amplitude increases only slightly), and the ripple structure has no correlation with the template nanocrystals (10−20 nm in size, inset in Figure 1). In fact, the ripple length is much longer than the grain size of the template; that is, they cross over many grains without significant change in the orientation. Therefore, it can be concluded that the grain boundaries of the nanocrystalline template can be transparent for surface diffusing atoms, justifying the absence of grain boundaries in our model. In this sense, our model is similar to that proposed for the island growth regime during Ag deposition on amorphous Si.[33]

Finally, we will discuss the origin of the anisotropic surface diffusion in our systems. In principle, for polycrystalline films formed mainly by randomly oriented grains, the existence of Erlich−Schwoebel barriers becomes improbable due to the lack of well-defined atomic steps at the surface. In this way, isotropic surface diffusivity rather than anisotropic is expected.[34] However, the experimental results clearly indicate the presence of anisotropy during deposition in the patterned surfaces and the simulations also point out that anisotropy is needed to organize the depositing material by surface diffusion. In this sense, this is one of the systems that exhibits this kind of behavior and whose origin remains unexplained, such as the elongated Ag island observed sometimes during evaporation of Ag on amorphized silicon (see Figure 1 in ref 33) and the growth of aligned Pt nanocrystals on Au(111) atomically smooth terraces (S. R. Brankovic, private communication). The cause of such anisotropy in surface diffusion is not evident and deserves a more detailed investigation. Whatever the origin for the anisotropy might be, it is worth analyzing if the proposed diffusion anisotropy involves a strong surface perturbation. According to the simulation shown above, we have seen that a ratio of probabilities $p = 0.2$ was enough to justify the occurrence of ripples. To make a qualitative argument, let us consider diffusion coefficients in two directions, say D_1 and D_2. According to a simple modeling in terms of state transition theory,[35] these diffusion coefficients could be written $D_i = D_i^0 e^{-E_1^{\#}}$, where D_i^0 shows a weak temperature dependence and $E_i^{\#}$ is the activation energy for the process. Thus, the ratio of diffusion coefficients can be approximated by $D_2/D_1 \approx e^{-(E_2^{\#} - E_1^{\#})/kT}$. Taking D_2/D_1 equal to 4 ($p = 0.2$), we find at 400 K that $E_2^{\#} - E_1^{\#} = 0.047$ eV. This value is only a small fraction (≈1%) of the binding energy of a typical d metal (3−5 eV). In other words, the present anisotropy may be explained with a minimal perturbation in the surface.

CONCLUSIONS

Ripples are spontaneously formed during deposition of metals, semiconductors, and alloys on different surfaces patterned with random arrays of nanocavities. Annealing of the template at relatively low temperatures also results in ripple formation. Both the experimentally determined nanocavity spacing and the simulated defect spacing determine the ripple wavelength before the final stage of coarsening. Therefore, nanocavities are able to guide the self-organization of these nanofeatures during their growth, creating the possibility for nanofabrication of parallel interconnections or circuits. On the other hand, ripple formation limits the use of nanocavities as reactors for nanocrystal growth to a narrow range of time (mass) and temperature. However, ripples are robust nanostructures that can also be used as templates for the preparation of hybrid nanostructured surfaces with specific physical properties.

METHODS

Gold and copper templates were prepared by physical vapor deposition on silane-modified nanostructured silicon masters with a surface array of short-range ordered nanodots prepared by Ar^+ irradiation (1.2 KeV) at normal incidence.[22] Dots are 40 nm in diameter and 6 nm in height, with a dot density ≈10^{11} cm^{-2}. The complete procedure for building the templates was described in ref 23. Briefly, the SiO_2 surface was chemically

modified by immersion in octadecyltrichlorosilane (OTS)-containing hexane solution for 1 h, forming a self-assembled silane monolayer. Afterward, 200 nm thick gold or copper films were deposited by thermal physical vapor deposition (PVD) on the OTS-covered silicon. The deposited polycrystalline metal films were mechanically detached from the OTS-covered master by using Scotch tape, due to the excellent anti-adherent properties of the silane monolayers.[23]

We have used gold templates containing a high density of nanocavities to deposit (a) copper, by electrodeposition from 1×10^{-3} M $CuSO_4 \cdot 5H_2O$ + 0.1 M H_2SO_4 at a linear potential sweep from $E = 0.000$ to 0.400 V (*vs* Cu^{2+}/Cu) at a temperature of $T = 298$ K, (b) silver, by electrodeposition from 1×10^{-3} M $AgNO_3$ + 0.5 M $HClO_4$ at a linear potential sweep from $E = 0.5$ to -0.04 V (*vs* Ag^+/Ag) at $T = 298$ K, and (c) NiFeCo alloy, a soft magnetic alloy, at $j = 20$ mA cm^{-2} from 0.06 M $CoSO_4 \cdot 7H_2O$ + 0.2 M $NiSO_4 \cdot 6H_2O$ + 0.015 M $FeSO_4 \cdot 7H_2O$ + 0.028 M NH_4Cl + 0.4 M H_3BO_3 + 2.6×10^{-4} M thiourea, pH 2.8 at 298 K.[36] On the other hand, copper templates were used to grow copper sulfide deposits (d) prepared by exposure of the copper templates to H_2S. In (c), the templates were modified with a self-assembled dodecanethiol monolayer prepared as reported in ref 32. This allows an easy release of the deposited film. The surface structures were characterized by scanning tunneling microscopy (STM) operating at constant current and atomic force microscopy (AFM) operating in the contact mode (Nanoscope IIIa Digital Instruments, Santa Barbara, CA).

Acknowledgment. The authors thank Bárbara Blum for her useful discussion. This work has been supported by ANPCyT (PICT05-32906, PICT06-621, PICT06-946, PAE 22711), CONICET (PIP 6075 and 5901), and UNLP (11/X425), Argentina.

REFERENCES AND NOTES

1. Timp, G. *Nanotechnology*; Springer-Verlag: New York, 1999.
2. Zhao, Z. M.; Xia, Y.; Whitesides, G. M. Soft Lithographic Methods for Nano-Fabrication. *J. Mater. Chem.* **1997**, *7*, 1069–1074.
3. Gates, B. D.; Xu, Q.; Stewart, M.; Deschner, R.; Willson, C. G.; Whitesides, G. M. New Approaches to Nanofabrication: Molding, Printing, and Other Techniques. *Chem. Rev.* **2005**, *105*, 1171–1196.
4. Erlebacher, J. D.; Aziz, M. J.; Chason, E.; Sinclair, M. B.; Floro, J. A. Non-Classical Smoothening of Nano-Scale Surface Corrugations. *Phys. Rev. Lett.* **2000**, *84*, 5800–5803.
5. Carter, G. Proposals for Producing Novel Periodic Structures on Silicon by Ion Bombardment Sputtering. *Vacuum* **2006**, *81*, 138–140.
6. Castro, M.; Cuerno, R.; Vazquez, L.; Gago, R. Self-Organized Ordering of Nanostructures Produced by Ion-Beam Sputtering. *Phys. Rev. Lett.* **2005**, *94*, 016102.
7. Nötzel, R.; Däweritz, L.; Ledentsov, N. N.; Ploog, K. Size Quantization by Faceting in (110)-Oriented GaAs/AlAs Heterostructures. *Appl. Phys. Lett.* **1992**, *60*, 1615–1617.
8. Krishnamurthy, M.; Wassermeier, M.; Williams, D. R. M.; Petroff, P. M. Periodic Faceting on Vicinal GaAs(110) Surfaces During Epitaxial Growth. *Appl. Phys. Lett.* **1993**, *62*, 1922–1924.
9. Ikarashi, N.; Baba, T.; Ishida, K. High-Resolution Transmission Electron Microscopy of Vicinal AlAs/GaAs Interfacial Structure. *Appl. Phys. Lett.* **1993**, *62*, 1632–1634.
10. Saito, H.; Uwai, K.; Tokura, Y.; Fukui, T. Step Ordering During Fractional-Layer Superlattice Growth on GaAs(001) Vicinal Surfaces by Metalorganic Chemical Vapor Deposition. *Appl. Phys. Lett.* **1993**, *63*, 72–74.
11. Pond, K.; Lorke, A.; Ibbetson, J.; Bressler-Hill, V. V.; Maboudian, R.; Weinberg, W. H.; Gossard, A. C.; Petroff, P. M. Step Bunching and Step Equalization on Vicinal GaAs(001) Surfaces. *J. Vac. Sci. Technol., B* **1994**, *12*, 2689–2693.
12. Cotta, M. A.; Hamm, R. A.; Staley, T. W.; Chu, S. N. G.; Harriott, L. R.; Panish, M. B.; Temkin, H. Kinetic Surface Roughening in Molecular Beam Epitaxy of InP. *Phys. Rev. Lett.* **1993**, *70*, 4106–4109.
13. Benson, J. D.; Almeida, L. A.; Carmody, M. W.; Edwall, D. D.; Markunas, J. K.; Jacobs, R. N.; Martinka, M.; Lee, U. Surface Structure of Molecular Beam Epitaxy (211)B HgCdTe. *J. Electron. Mater.* **2007**, *36*, 949–957.
14. Lee, N.-E.; Cahill, D. G.; Greene, J. E. Surface Roughening During Low-Temperature Si Epitaxial Growth on Singular *vs* Vicinal Si(001) Substrates. *Phys. Rev. B* **1996**, *53*, 7876–7879.
15. Carbone, D.; Alija, A.; Plantevin, O.; Gago, R.; Facsko, S.; Metzger, T. H. Early Stage of Ripple Formation on Ge(001) Surfaces Under Near-Normal Ion Beam Sputtering. *Nanotechnology* **2008**, *19*, 035304–035308.
16. Bracco, G.; Cavanna, D. Decay of Nanoripples on Au(111) Studied by He Atom Scattering. *Phys. Rev. B* **2007**, *76*, 033411−033414.
17. Rusponi, S.; Costantini, G.; Boragno, C.; Valbusa, U. Ripple Wave Vector Rotation in Anisotropic Crystal Sputtering. *Phys. Rev. Lett.* **1998**, *81*, 2735–2738.
18. Pedemonte, L.; Bracco, G.; Boragno, C.; Buatier de Mongeot, F.; Valbusa, U. He Diffraction Study of the Time Decay of Ripple Structures on Ion Bombarded Ag(110). *Appl. Surf. Sci.* **2003**, *212−213*, 344–348.
19. Mishra, P.; Ghose, D. Formation of Nanoripples in Al Films During O_2^+ Sputtering. *Phys. Rev. B* **2006**, *74*, 155427–155432.
20. Gago, R.; Vázquez, L.; Cuerno, R.; Varela, M.; Ballesteros, C.; Albella, J. M. Nanopatterning of Silicon Surfaces by Low-energy Ion-beam Sputtering: Dependence on the Angle of Ion Incidence. *Nanotechnology* **2002**, *13*, 304–308.
21. dos Santos Claro, P. C.; Fonticelli, M.; Benítez, G.; Azzaroni, O.; Schilardi, P. L.; Luque, N. B.; Leiva, E.; Salvarezza, R. C. Silver Electrodeposition on Nanostructured gold: from Nanodots to Nanoripples. *Nanotechnology* **2006**, *17*, 3428–3435.
22. Gago, R.; Vázquez, L.; Cuerno, R.; Varela, M.; Ballesteros, C.; Albella, J. M. Production of Ordered Silicon Nanocrystals by Low-Energy Ion Sputtering. *Appl. Phys. Lett.* **2001**, *78*, 3316.
23. Azzaroni, O.; Fonticelli, M.; Benítez, G.; Schilardi, P. L.; Gago, R.; Caretti, I.; Vázquez, L.; Salvarezza, R. C. Direct Nanopatterning of Metal Surfaces through Self-Assembled Molecular Films. *Adv. Mater.* **2004**, *16*, 405–409.
24. Guan, Y. F.; Pedraza, A. J. Synthesis of Aligned Nanoparticles on Laser-Generated Templates. *Nanotechnology* **2005**, *16*, 1612–1618.
25. Oates, T. W. H.; Keller, A.; Facsko, S.; Mücklich, A. Aligned Silver Nanoparticles on Rippled Silicon Templates Exhibiting Anisotropic Plasmon Absorption. *Plasmonics* **2007**, *2*, 47–50.
26. Sánchez, C. G.; Leiva, E. P. M.; Kohanoff, J. The Relevance of Heterometallic Binding Energy for Metal Underpotential Deposition. *Langmuir* **2001**, *17*, 2219–2217.
27. Nanda, K. K.; Maisels, A.; Kruis, F. E.; Rellinghaus, B. Anomalous Thermal Behaviour of Gold Nanostructures. *Europhys. Lett.* **2007**, *80*, 56003-p1–56003-p4.
28. Heermann, D. W. *Computer Simulation Methods in Theoretical Physic*; Springer-Verlag: Heidelberg, 1989.
29. Lavis, D. A.; Bell, G. M. *Statistical Mechanics of Lattice Systems*; Springer-Verlag: Heidelberg, 1999; Vol. 1.
30. Kang, H. C.; Weinberg, W. H. J. Dynamic Monte Carlo with a Proper Energy Barrier: Surface Diffusion and Two-Dimensional Domain Ordering. *J. Chem. Phys.* **1989**, *90*, 2824–2830.
31. Kawasaki, K. Diffusion Constants Near the Critical Point for Time-Dependent Ising Models. I. *Phys. Rev.* **1966**, *145*, 224–230.
32. Rost, M. J. *In Situ* Real-Time Observation of Thin Film Deposition: Roughening, Zeno Effect, Grain Boundary Crossing Barrier and Steering. *Phys. Rev. Lett.* **2007**, *99*, 266101-1–266101-4.

33. Polop, C.; Rosiepen, C.; Bleikamp, S.; Drese, R.; Mayer, J.; Dimyati, A.; Michely, T. The STM View of the Initial Stages of Polycrystalline Ag Film Formation. *New J. Phys.* **2007**, *9*, 74.
34. Muñoz-García, J.; Vazquez, L.; Cuerno, R.; Sanchez-García, J. A.; Castro, M.; Gago, R. Self-Organized Surface Nanopatterning by Ion Beam Sputtering. In *Lecture Notes on Nanoscale Science and Technology*; Wang, Z., Ed.; Springer: Heidelberg, in press, ArXiv:0706.2625v1.
35. Hill. T. L. *An Introduction to Statistical Thermodynamics*; Dover Publications Inc.: New York, 1987.
36. Azzaroni, O.; Schilardi, P. L.; Salvarezza, R. C. Templated Electrodeposition of Patterned Soft Magnetic Films. *Appl. Phys. Lett.* **2002**, *80*, 1061–1063.